Cancer Immunology, Immunotherapy (2025) 74:44
https://doi.org/10.1007/s00262-024-03889-x

RESEARCH

Fractionated low-dose radiotherapy primes the tumor microenvironment for immunotherapy in a murine mesothelioma model

Rebecca A. D'Alonzo[1,2,3] · Synat Keam[2,3,4] · Suki Gill[1,4,5] · Pejman Rowshanfarzad[1] · Anna K. Nowak[2,3,4] · Martin A. Ebert[1,5] · Alistair M. Cook[2,3,6]

Received: 30 July 2024 / Accepted: 9 November 2024

Abstract

Combination immune checkpoint inhibitors (nivolumab and ipilimumab) are currently a first-line treatment for mesothelioma; however, not all patients respond. The efficacy of treatment is influenced by the tumor microenvironment. Murine mesothelioma tumors were irritated with various radiotherapy doses. Radiotherapy induced vasculature changes were monitored by power Doppler and photoacoustic ultrasound and analyzed via mixed-effects models. Tissue staining was used to investigate the immune cell infiltrate of tumors. The optimal radiotherapy schedule was combined with immune checkpoint inhibitors, and the survival of mice was analyzed. Using low-dose, low-fraction radiotherapy allowed favorable modification of the murine mesothelioma tumor microenvironment. Irradiating tumors with 2 Gy × 5 fractions significantly improved blood flow and reduced hypoxia, consequently increasing the presence of $CD8^+$ and regulatory T cells in the tumor. Understanding the transient nature of these changes is crucial for optimizing the timing of therapeutic delivery. The combination of radiotherapy with dual immunotherapy (anti-PD-1 plus anti-CTLA-4) proved highly curative when administered concurrently. A diminishing rate of cures was noted with an increasing delay between radiotherapy and subsequent immunotherapy. Concurrent low-dose, low-fraction radiotherapy emerges as a translatable approach for improving the efficacy of immune checkpoint inhibitors in patients.

Keywords Tumor microenvironment · Vasculature remodeling · Low-dose radiotherapy · Immunotherapy

Introduction

Only a subset of cancer patients (13–43%) receiving immune checkpoint inhibitors (ICIs) experience therapeutic benefit [1, 2]. Poor responses partly result from impediments in the tumor microenvironment (TME), including abnormal and dysfunctional vasculature [3–7]. Disorganized vessels exhibit excessive branching, arteriovenous shunts, and weakened vessel walls, creating regions of hypoxia and acidity [4–8]. Hypoxia can upregulate genes associated with angiogenesis, glycolysis, metastasis, and tumor progression [4–8]. Hypoxia increases immune checkpoint molecules, including programmed death-ligand 1 (PD-L1), and increases immunosuppressive cells, such as tumor-associated macrophages and regulatory T cells (Tregs) — resulting in impaired immune cell function [6, 7]. Some hypoxia-associated factors are found not only in the TME, but also in peripheral circulation, promoting systemic immunosuppression and facilitating metastatic spread [6, 7]. Poor perfusion, leaky vessels,

Rebecca A. D'Alonzo and Synat Keam have equally contributed to this work.

✉ Rebecca A. D'Alonzo
rebecca.dalonzo@uwa.edu.au

✉ Alistair M. Cook
alistair.cook@uwa.edu.au

1 School of Physics, Mathematics and Computing, The University of Western Australia, Perth, Australia

2 National Centre for Asbestos Related Diseases, The University of Western Australia, Perth, Australia

3 Institute for Respiratory Health, Perth, Australia

4 Medical School, The University of Western Australia, Perth, Australia

5 Department of Radiation Oncology, Sir Charles Gairdner Hospital, Perth, Australia

6 School of Biomedical Sciences, The University of Western Australia, Perth, Australia

Published online: 03 January 2025

and dysfunctional supporting cells also inhibit circulating drugs and immune cells from entering tumors and enable cancerous cells to access the blood stream [6–8]. Abnormal vascular growth, hypoxia, and immunosuppression are intricately linked through complex feedback processes.

Low-dose radiotherapy (LDRT; small numbers of fractions ≤ 2 Gy per fraction, resulting in a low total dose) may enhance tumor perfusion and oxygenation through vascular normalization [7–13]. LDRT also modulates TME immune components, which leads to effector T cell recruitment and activation of $CD4^+$ T cells, $CD8^+$ T cells, Tregs, myeloid cells, and other immune cells [13–19]. LDRT induces upregulation of immune checkpoint molecules on tumor cells, including PD-L1 [13, 18–20]. The immuno-modulatory effects of LDRT typically last for a week, with repeated treatments sustaining these effects [15–18, 20]. Vascular remodeling can persist for up to two weeks post-irradiation in mice [8–11, 13, 21], and potentially longer in patients [13, 22, 23]. Compared to single-dose RT, fractionation improves extravascular normalization, perfusion, oxygenation [7, 9, 10, 13], and increases immune cell infiltration [13, 24, 25]. LDRT-induced TME modulation can synergize with various immunotherapies [14–17, 20, 26, 27], with fractionated RT yielding better treatment outcomes over single-dose RT when combined with ICIs [13, 25]. Windows of LDRT-induced vascular normalization and immune response may have more predictable timing than anti-angiogenic drugs; even for different tumor types [13, 15]. Despite this, optimal LDRT dose fractionation and respective timing of immunotherapy remain unclear. A few days delay in delivering immunotherapy following LDRT can significantly reduce treatment response [19, 20, 25, 26]. However, other studies have indicated a broader time range in which positive outcomes can still be achieved [15, 19, 26]. Thus, the optimal timing of LDRT-immunotherapy combination varies with factors such as RT dose, fractionation, immunotherapies used (including single versus dual immunotherapies), and tumor type — leading to a range of responses. Investigation into temporal changes within the TME, and its immune component, will help define the normalization window and can guide the timing of ICI delivery.

Mesothelioma, a typical cancer for ICI treatment, has a clinically approved first-line treatment of anti-CTLA-4 (ipilimumab) and anti-PD-1 (nivolumab), but response rates remain low [28]. Here, we investigate the potential of LDRT to normalize tumor vasculature and examine variations in both vascular and immunological aspects within the TME. Using novel in vivo imaging technology and immunohistochemistry, we tracked temporal changes in vasculature, hypoxia, and immune infiltrate. These approaches allow for identification of optimal LDRT fractionation schedules to prime tumors for immunotherapy. Finally, a successful, highly curative radiotherapy-immunotherapy combination in a preclinical mesothelioma mouse model is reported, using ICIs analogous to current first-line clinical mesothelioma treatment.

Materials and methods

Mice

Female BALB/cJAusBP mice (aged 6–8 weeks) were obtained from Harry Perkins Institute of Medical Research (HPIMR) South Facility (Perth, Australia) and housed at HPIMR North Facility (Perth, Australia). All mouse experiments were approved by the respective authorities and conducted in accordance with the Australian Code for the Care and Use of Animals for Scientific Purposes (8th edition, 2013) and University of Western Australia animal ethics guidelines and protocols.

Cell lines

The AB1-HA cell line was obtained from the National Centre for Asbestos Related Diseases (NCARD; Perth, Australia). AB1 murine mesothelioma cell lines were originally generated by intraperitoneal injection of crocidolite asbestos into BALB/c mice [29, 30] and then transfected with influenza hemagglutinin (HA) to generate the AB1-HA cell line [31]. Cells were cultured in a medium containing 20 mM N-2-hydroxyethylpiperazine-N'-2-ethanesulfonic acid (HEPES; Sigma Aldrich, Australia), 100U/mL Benzylpenicillin, 500 mg/mL Gentamicin, 0.05 mM 2-Mercapteothanol, and 10% neonatal calf serum.

Tumor model

AB1-HA cells were resuspended in sterile 1X phosphate-buffered saline (PBS) at 5×10^6 cells/mL, 100 µL (5×10^5 cells) was then subcutaneously injected into the shaved right flank (designated 'day 0'). Tumor width (W) and length (L) were measured using calipers, tumor volume was calculated using the formula $(W^2 \times L)/2$. Mice were euthanized at specified time points as indicated, or sooner if tumors reached the maximum volume of $1000mm^3$ before the time point indicated.

Radiotherapy

Tumor irradiation was conducted using the Precision X-Ray Small Animal Radiation Therapy (SmART) X-RAD225Cx, utilizing Pilot software (version 1.12) and SmART-Plan

software (version 2.0) (Precision X-Ray, Connecticut, USA). The device is calibrated according to the AAPM protocols [32], with technical details provided in Feddersen, 2019 [33]. Radiotherapy was performed with a 225 kVp beam, 13 mA tube current, dose rate of 3 Gy/min, and a source to target distance of approximately 30 cm. Treatment plans were individualized for each mouse at each time point, created from a cone beam CT taken each treatment day. Treatment plans had a single isocenter in the middle of the tumor. Two fixed coplanar beams, 180° apart, each delivered half of the prescribed dose via the sagittal plane. Tumors were irradiated with a 5 mm diameter circle collimator. Mice were anesthetized (1.5–2% isoflurane in 100 mL/min air) for a total time of 15–20 min, which included positioning, CT imaging, and irradiation; animals not receiving RT (sham-irradiation) were anesthetized for a comparable duration. RT time points are provided in Figs. 1a, 3a, and 6a.

Immunotherapy

ICI antibodies used in this study were anti-PD-1 (clone RMP1-14, Rat IgG2a) and anti-CTLA-4 (clone 9H10, Syrian Hamster IgG), obtained from BioXcell (West Lebanon, NH, USA). A total of 200 µg of each antibody were suspended in 100 µl of InVivoPure pH 7 sterile dilution buffers (Cat # IP0070, BioXcell, New Hampshire, USA) and administered via intraperitoneal injection. Control mice were injected with 100 µl dilution buffer. ICI time points are provided in Fig. 6a.

Ultrasound imaging

Ultrasound imaging was performed using a Vevo LAZR-X High Frequency Ultrasound and Photoacoustic Imaging system (Fujifilm VisualSonics, Toronto, Canada). An MX550D transducer was used for power Doppler (gain: 40 dB) and photoacoustic ultrasound imaging (gain: 40 dB). Employing the Vevo Rail system (Fujifilm, VisualSonics, Inc.), a 3D scan of the whole tumor was conducted with a step size of 0.05 mm. Imaging with both modalities (anesthetized with 1.5–2% isoflurane in 100 mL/min air for 20 min), occurred every second day, commencing day 15 post-inoculation and maintained to day 29 or euthanasia. Ultrasound time points are provided in Fig. 1a.

Image analysis

Ultrasound images were imported into VevoLab Analysis software (version 5.5.1) (Fujifilm VisualSonics, Toronto, Canada). The largest 25% of the tumor was contoured, as determined by the area in the transverse plane. Core volumes, a 1 mm diameter circle in the center of the tumor, were also contoured. The 'whole core' extends to the previously contoured tumor slices, and the 'center core' consists of 11 slices centered in the largest contoured area. Slices displaying breathing artifacts were excluded. The software calculated the percentage of functional vasculature blood flow ($\%V_{flow}$) from power Doppler images and oxygen saturation ($\%sO_2$) values from photoacoustic images. Data, including pixels without a photoacoustic signal, were used to calculate $\%sO_2$ levels in overall tumor tissue ($\%sO_2T$), and blood $\%sO_2$ ($\%sO_2B$) values were calculated using only pixels with a photoacoustic signal.

Immunohistochemistry

Tumors were collected at time points specified in figure legends and were frozen in OCT compound buffer (Thermofisher Scientific, Massachusetts, USA). Sections 7 µm thick were stained using various antibodies (Supplementary Table 1) and DAPI nuclear stain. Sections were examined by PANNORAMIC 250 Flash III slide scanner (Budapest, Hungary). The percentage of area positive for markers, or T cell concentration, were calculated using HistoQuant and CellQuant (Budapest, Hungary), respectively. Vessel diameter was measured by manually outlining individual groups of conjoined $CD31^+$ cells ('vessels'), then HistoQuant software used to calculate the average diameter of that vessel. A mean vessel diameter was then calculated from all $CD31^+$ vessels in any given tumor section. The vessel density was counted as the number of vessels per 1 mm^2. At least three sections per tumor analyzed. For functional analysis, mice were injected with pimonidazole (intraperitoneal injection, 60 mg/kg, 60 min prior to euthanasia), and/or lectin-FITC (intravenous injection, 50 µg/mouse, 10 min prior to euthanasia).

RNA extraction and sequencing

Tumors were collected on days 14, 15, 18, 22, and 27 post-inoculation (Fig. 3a) and RNA extracted using a RNeasy Kit with RNeasy Mini Spin Columns (QIAGEN, Maryland, USA) according to manufacturer's instructions. RNA was quality checked using a Bioanalyzer (Agilent) and stored at -80 °C before sequencing. Total RNA libraries were prepared using TruSeq Stranded mRNA library Prep Kit (Illumina Inc., California, USA) and sequenced by Illumina HiSeq2500, 50 bp paired reads, v4 chemistry, at the Australian Genome Research Facility. On average, 20 million reads were generated per sample.

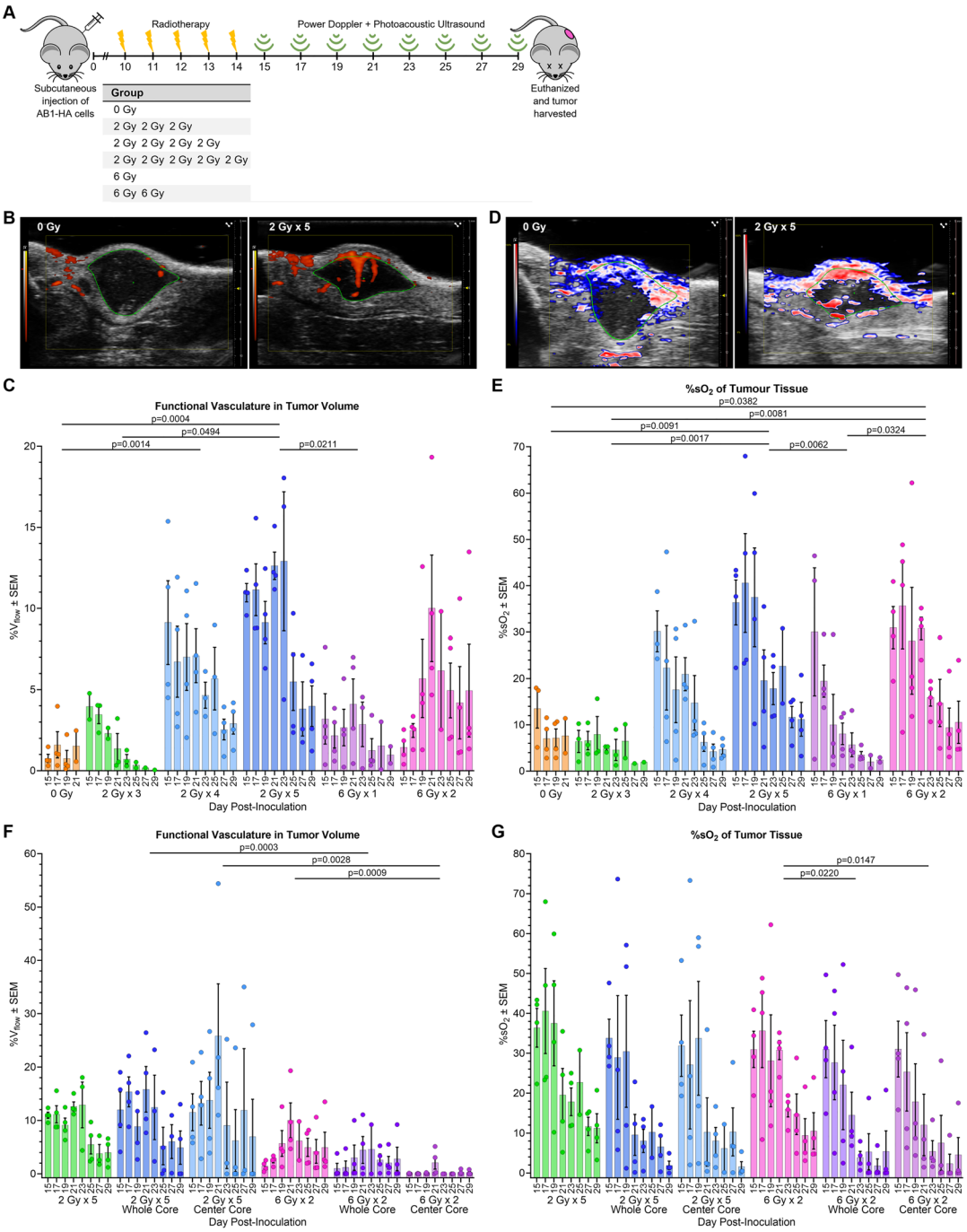

RNAseq analysis

Quality of RNA sequencing raw files were assessed using FastQC, then aligned to mouse reference genome using Kallisto [34], with more than 90% of reads mapped to the reference genome. Gene level quantification (count) of aligned reads was performed using the tximport function in R [35], genes with < 10 counts were removed. Principal component analysis was performed using variance stabilizing transformation, and analysis of differentially expressed genes between groups was carried out using DESeq2 [36]. Gene Ontology and hallmark pathway analyses were performed using Enrichr, and significant pathways (overrepresentation) were examined using Fisher's exact test [37]. Estimation of the proportion of infiltrating immune cells from the normalized count of bulk-RNA sequencing data was performed using the CIBERSORT algorithm [38], based on the 511-mouse gene signature as a reference [39] and was validated for 25 mouse immune cell types.

◂**Fig.1** LDRT increases the functional vasculature and oxygen saturation in tumors. **A** Schematic showing the experimental timeline. Subcutaneous injection of AB1-HA mesothelioma cells on day 0. Radiotherapy commenced on day 10 post-inoculation when tumors were ~ 40 mm^3 (standard deviation ± 15 mm^3). Each group received dose and fraction as stated in the table. Power Doppler and photoacoustic imaging commenced the day following final irradiation (day 15) and was conducted every second day until tumors reached 1000 mm^3 or until the experimental endpoint on day 29. **B** Representative Power Doppler ultrasound of non-irradiated (0 Gy) tumor (0.3%V_{flow} day 15) and irradiated (2 Gy × 5) tumor (15.3%V_{flow} day 23) of similar contoured volumes (21.5 ± 1.5 mm^3). **C** Analysis of power Doppler ultrasound to determine the %V_{flow} of the contoured tumor volume. Results show the mean %V_{flow} ± standard mean error (SEM) for each group at each time point with individual data points shown. **D** Representative photoacoustic ultrasound of non-irradiated (0 Gy) tumor (17.5%sO_2T and 40.1%sO_2B day 15) and irradiated (2 Gy × 5) tumor (22.6%sO_2T and 66.7%sO_2B day 23) of similar contoured volumes (26.5 ± 2.6 $mm.^3$). **E** Analysis of photoacoustic ultrasound to determine the %sO_2T of the contoured tumor volume. Results show the mean %sO_2T ± SEM plus individual data points for each group at each time point. **F** Comparison of the %V_{flow} in the whole contoured tumor volume and the center tumor volume for 2 Gy × 5 fractions (LDRT) and 6 Gy × 2 fractions (hypofractionated dose). **G** Comparison of the %sO_2T of the whole contoured tumor volume and the center tumor volume for 2 Gy × 5 fractions and 6 Gy × 2 fractions. P values calculated using estimated marginal means with Tukey's adjustment, based on mixed-effect model. The experiment was repeated 4 times, with 1 mouse from each group in each experimental repeat (n = 4 mice per group), except for the 2 Gy × 3 group where n = 3 mice per group. Not all days have 4 imaging data points; this is due to equipment error. The 0 Gy, 2 Gy × 3, and 6 Gy × 1 fraction groups had mice reach the maximum tumor volume and were euthanized before day 29 post-inoculation (0 Gy: 2 mice day 19 and 2 day 21. 2 Gy × 3: 1 mouse day 23 and 1 day 25. 6 Gy × 1: 2 mice day 25)

Tumor rechallenge

'Cured' mice (tumor-free for 30 days) were reinoculated with subcutaneous injection (5×10^5 AB1-HA cells in 100 µl PBS) on the opposite flank and monitored until 80 days post-primary tumor inoculation. In each batch of rechallenge injections, five naïve control mice also received inoculation for quality control (data not shown).

Statistical analysis

For all experiments, mice were randomized into groups and investigators were not blinded. Sample sizes were calculated using power and sample size calculation software [40]. For experiments involving matched data and repeated imaging, a group size of four mice provided 80% power ($p = 0.05$) to detect 40% change, considering a 20% standard deviation. The same group size was adopted for the time-course immunohistochemistry. For radiotherapy-immunotherapy investigation, ten mice per group were initially planned to detect a 26% difference between schedules with 80% power ($p = 0.05$), assuming a 20% within-group standard deviation. In the event a tumor showed delayed growth and was too small at the beginning of the experiment (< 15 mm^3 on day 10 post-inoculation); these mice were excluded from treatment prior to randomization. This reduced the number of mice per group to a minimum of seven, resulting in a detectable difference of 32% using the same parameters of power and significance as above. The number of mice and replicates are specified in each figure legend.

Statistical analyses used R software (R Studio version 4.1.2). In the RT dose titration experiment, multiple group comparisons for imaging modalities were performed using linear mixed-effects models. Considering the longitudinal nature of the data and the relationship between measurements and the day post-inoculation, it was necessary to control for several factors, including experimental group, contoured area, post-inoculation time point, and interactions between these variables. Additionally, a random factor was included in the model to account for variations between individual mice. Multiple group comparisons from final models were performed using estimated marginal means (EMMs) with Tukey's adjustment. This was used to compare group means for each modality/model. For pairwise comparison of groups given the same tumor area, EMMs with Tukey's adjustment were set to assess the model at given areas (5–50 mm^2). The same analysis method was used to compare imaging days. Multiple group comparisons for tissue stains from RT dose titration experiments were performed using one-way analysis of variance (ANOVA) with Tukey's adjustment for pair-wise comparison. A two-group comparison of tissue stains from the time-course study was performed using an independent T test (RT and size-matched sham-irradiation). A linear mixed-effects model was used to compare tumor growth between groups. The Kaplan-Meier method was used to estimate survival curves, and log-rank statistics used to compare survival between groups. Statistical significance was set at $p < 0.05$.

RESULTS

Fractionated low-dose RT increases blood flow and oxygen saturation in tumors

Low-dose radiotherapy (LDRT; small numbers of fractions ≤ 2 Gy per fraction resulting in a low total dose) has been postulated to normalize tumor vasculature and reduce hypoxia [7–13]. However, this area of research remains poorly studied-particularly regarding optimal RT dosing and scheduling, and the mechanisms underlying these effects. We titrated the number of 2 Gy fractions required to achieve vascular remodeling in subcutaneous AB1-HA mesothelioma tumors. These treatment schedules were also compared to hypofractionated (6 Gy) treatments and sham-irradiated controls (Fig. 1a). Temporal changes in

response to RT schedules were tracked by imaging tumors on alternate days post-irradiation using power Doppler and photoacoustic ultrasound, allowing measurement of both inter- and intra-tumor variability [41].

A significant increase in blood flow ($\%V_{flow}$) was observed in tumors treated with 2 Gy × 5 fractions and 2 Gy × 4 fractions compared to non-irradiated controls (Fig. 1b and 1c). Tumors receiving 2 Gy × 5 fractions and 2 Gy × 4 fractions exhibited a mean blood flow increase of 10.5 and 7.5 times compared to controls, respectively. The 2 Gy × 5 fractions group achieved maximum $\%V_{flow}$ 21–23 days post-inoculation (i.e.,7–9 days after final irradiation) (Fig. 1c). Tumors receiving 2 Gy × 4 or 2 Gy × 5 fractions continued to have significantly higher $\%V_{flow}$ compared to non-irradiated tumors at all time points. To check whether these changes were not simply correlated with tumor size, comparisons were made between tumors of the same contoured area, confirming that tumors treated with 2 Gy × 4 or 2 Gy × 5 fractions exhibited significantly higher $\%V_{flow}$ than the controls (Supplementary Fig. 1a).

To examine inter-tumor and intra-tumor changes in oxygen saturation ($\%sO_2$), tumors were imaged using photoacoustic ultrasound (Fig. 1a). Photoacoustic imaging uses the differential absorption properties of oxygenated and deoxygenated hemoglobin to calculate the $\%sO_2$ of the total tumor tissue volume ($\%sO_2T$) and blood ($\%sO_2B$) [41]. The $\%sO_2T$ in tumors treated with 2 Gy × 5 and 6 Gy × 2 fractions significantly increased compared to the control group (Fig. 1d and 1e). Tumors receiving 2 Gy × 5 or 6 Gy × 2 fractions had a mean $\%sO_2T$ that was 4 and 3.5 times greater than non-irradiated tumors during the same imaging session, respectively. Maximum $\%sO_2T$ values were sustained until 19 days post-inoculation (5 days post-irradiation) for tumors that received 2 Gy × 5 fractions (Fig. 1e). Although there was a decreasing trend in $\%sO_2T$ over time, both the 2 Gy × 5 and 6 Gy × 2 fraction groups had greater $\%sO_2T$ than the sham-irradiated group on all days. When comparing established tumors of equivalent size (contoured area > 15 mm^2), 2 Gy × 5 and 6 Gy × 2 fractions resulted in significantly higher $\%sO_2T$ than non-irradiated groups (Supplementary Fig. 1b). Significant increases in $\%sO_2B$ were observed in tumors treated with 2 Gy × 4 fractions and 2 Gy × 5 fractions compared to the sham-irradiated group (Supplementary Fig. 2). Tumors that received 2 Gy × 4 and 2 Gy × 5 fractions both had 1.4 times greater $\%sO_2B$ than non-irradiated tumors (Supplementary Fig. 2). The $\%sO_2B$ for the 2 Gy × 5 fractions group remained stable over time, suggesting the functionality of blood vessels was maintained over time. The 2 Gy × 4 fractions and 2 Gy × 5 fractions groups exhibited greater $\%sO_2B$ than the control group across all time points (Supplementary Fig. 2) and for all areas (Supplementary Fig. 1c).

Although LDRT and hypofractionated RT resulted in similar sized tumors (Supplementary Fig. 1d), there were regional differences between the doses, thus the core data was analyzed. We found that 2 Gy × 5 fractions significantly increased blood flow in the middle of tumors compared to those treated with 6 Gy × 2 fractions (Fig. 1f). For 6 Gy × 2 fractions, there was a significant decrease in $\%sO_2T$ in the middle of the tumor (Fig. 1g). Analysis of $\%sO_2B$ found no significant difference in irradiated tumor regions for both intra-group and inter-group comparisons (Supplementary Fig. 2b). Tumor growth curves are shown in Supplementary Fig. 1d.

When mice were euthanized (time points specified in Fig. 1a) tumors were collected for immunofluorescence staining. Analysis of endothelial ($CD31^+$) cells revealed that only the 2 Gy × 5 fraction group had significantly smaller and thinner vessels compared to non-irradiated controls (Fig. 2a–d) — more characteristic of 'normal' blood vessels found in non-tumor tissues [42]. Higher concentrations of $CD3^+$ T cells were observed in tumors irradiated with 2 Gy × 5 fractions than sham-irradiated tumors (Fig. 2e and 2f). The mean diameter of intra-tumor blood vessels was inversely correlated with T cell concentration (Supplementary Fig. 3).

Low-dose RT transiently alters functionality and morphology of tumor vasculature

Herein, the study focused on 2 Gy × 5 fractions, as this schedule resulted in the greatest increase in tumor blood flow, $\%sO_2$, and $CD3^+$ T cell concentration, which were sustained for a week post-irradiation. Lower doses per fraction (i.e., 2 Gy vs. 6 Gy) would minimize potential damage to endothelial cells and pre-existing T cells within the tumor. To gain further insights into temporal effects of 2 Gy × 5 fractions on the TME, a time-course study was conducted by harvesting tumors at different post-irradiation timepoints (Fig. 3a). Lectin (a surrogate for vascular perfusion) revealed a significant increase in lectin-stained vessels within LDRT (2 Gy × 5) tumors 3 h (0.1 day), 1 day, and 4 days post-irradiation. By day 8, perfusion returned to levels similar to those in untreated tumors, indicating transient vascular normalization (Fig. 3b and 3c). Hypoxia, assessed using pimonidazole staining, showed that the proportion of hypoxic areas within tumors were significantly lower in the LDRT group compared to sham-irradiated controls 0.1-, 1-, and 4-days post-irradiation; however, by day 8 hypoxia had increased to non-irradiated equivalent levels (Fig. 3d and 3e). These results further indicate that LDRT transiently restored vascular function, improved vessel perfusion and reduced tumor hypoxia.

To further characterize short-term LDRT-induced vascular changes, sections collected 1-day post-irradiation

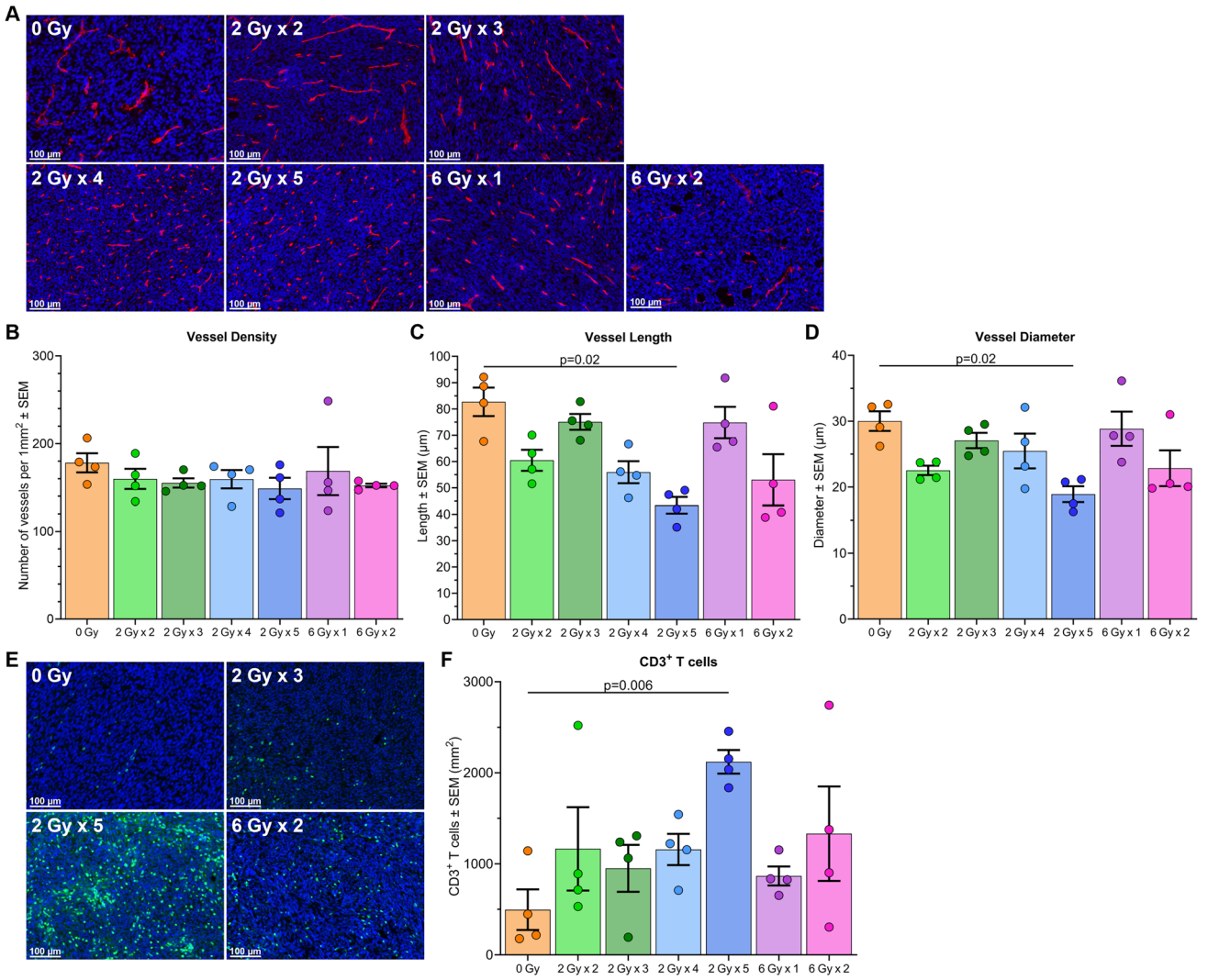

Fig. 2 LDRT reduces vessel length and diameter and increases intratumoral $CD3^+$ T cells. **A** Representative immunofluorescence images of endothelial cells ($CD31^+$, red) from mesothelioma tumors treated with various RT fractionation schedules. **B-D** Mean data plus individual data points showing vessel density, length, and diameter. **E** Representative immunofluorescence images of sectioned tumor tissue from mesothelioma tumors treated with various RT fractionation schedules, stained for T cells ($CD3^+$, green). **F** Mean data plus individual data points displaying $CD3^+$ T cells per unit area ($mm.^2$). P values calculated using one-way analysis of variance (ANOVA) with Tukey's adjustment. The experiment was repeated 4 times, with 1 mouse from each group in each experimental repeat (n = 4 mice per group)

underwent additional staining. This time point was chosen as it had the largest difference in hypoxia and perfusion between the irradiated versus non-irradiated tumors. Pericyte cells were evaluated using alpha smooth muscle actin (aSMA), and pericyte integrity via the perivascular markers calponin and caldesmon [10, 21, 42]. LDRT (2 Gy × 5) increased pericyte coverage around blood vessels compared to the non-irradiated group (Fig. 3f). Although the proportion of caldesmon covering the tumor vessels appeared elevated in the LDRT group (suggesting pericyte maturation) compared to the sham-irradiated group, the difference was not significant ($p = 0.09$; Fig. 3g). There was no significant difference in calponin expression, which serves as a marker of pericyte contractile ability (Fig. 3h). Endothelial cell activation enables effective T cell migration to the tumor [5]. To examine whether LDRT could activate endothelial cells and strengthen the basement membranes around the vessels, tumor sections were stained with ICAM-1 and collagen-IV, respectively. LDRT resulted in increased ICAM-1 compared to controls (Fig. 3i), suggesting endothelial cell activation However, there was no significant difference in collagen-IV expression, suggesting little change in blood vessel basement membranes between the LDRT and non-irradiated groups (Fig. 3j).

Following the earlier observation of increased $CD3^+$ T cells two weeks after LDRT, tumor sections were stained for

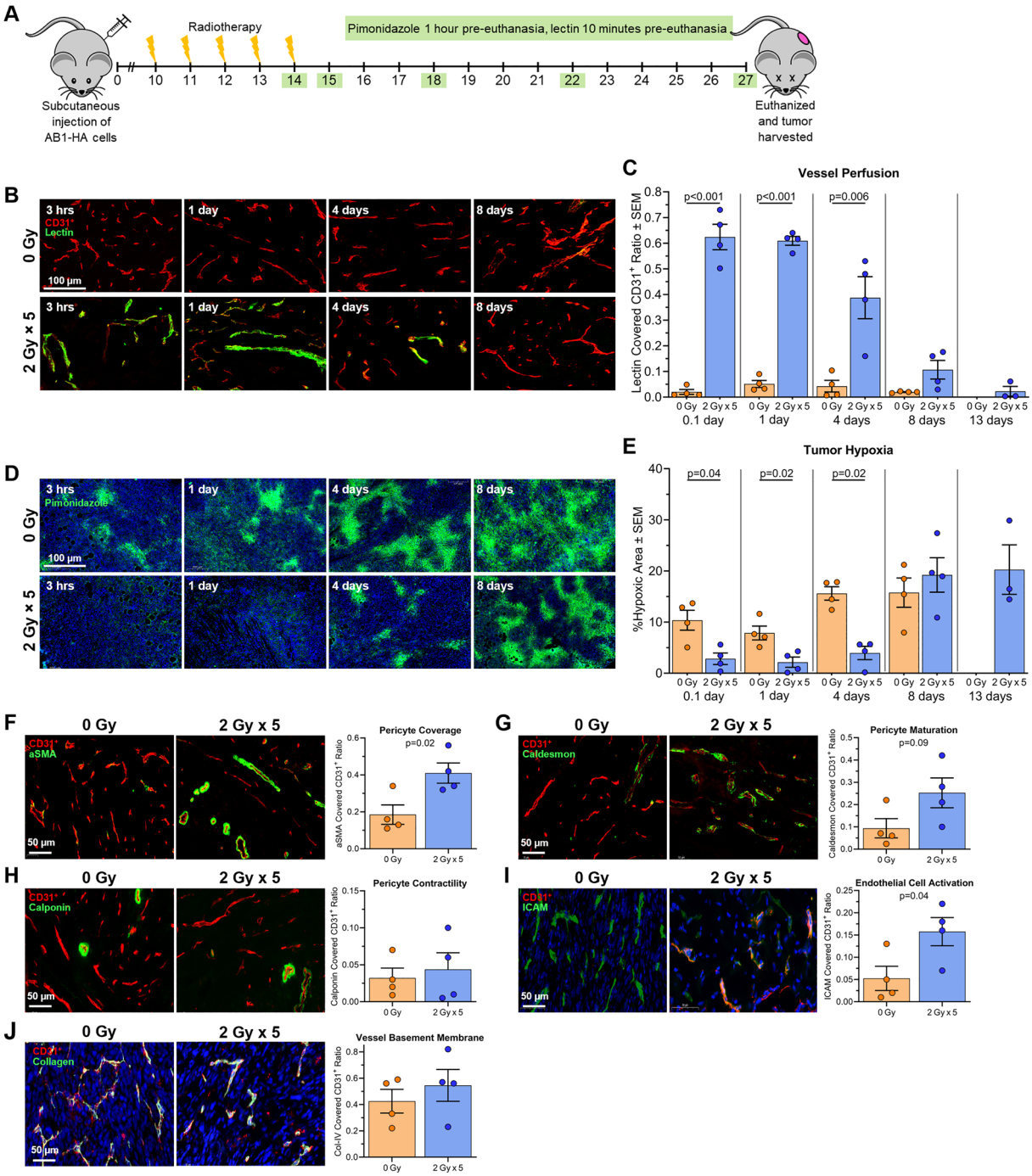

CD8$^+$ T cells and Tregs (Foxp3$^+$) at all time points (Fig. 3a). CD8$^+$ T cell numbers were significantly higher in tumors receiving LDRT than in sham-irradiated tumors from 1 to 4 days post-irradiation, then plateauing until the final time point (Fig. 4a and 4c). Additionally, Foxp3$^+$ Tregs were more numerous in LDRT tumors compared to the control groups (Fig. 4b and 4d). Although CD8$^+$ to Treg ratios showed an increasing trend in favor of CD8$^+$ cells in the LDRT group compared to the non-irradiated group, the differences were not statistically significant (Fig. 4e).

Low-dose RT upregulates inflammatory pathway genes and modulates the immunological environment

To investigate changes in gene expression induced by LDRT (2 Gy × 5), bulk-RNA sequencing was conducted on tumors collected 0.1, 1-, 4-, and 8-days post-irradiation (Fig. 3a). Principal component analysis revealed that RNA transcripts from LDRT groups were separated from non-irradiated tumors (Fig. 5a). Analysis showed that tumors collected

◂**Fig. 3** LDRT decreases hypoxia, increases perfusion and pericyte coverage, and activates tumor blood vessels. **A** Schematic showing time-course experimental plan. Subcutaneous injection of AB1-HA mesothelioma cells at day 0. Radiotherapy commenced on day 10 post-inoculation when tumors were ~ 40 ± 15 mm^3. At each experimental time point (green box) mice were injected with pimonidazole and lectin prior to euthanasia; tumors were subsequently removed for analysis. Untreated mice were euthanized on day 22 post-inoculation (when maximum tumor volume reached), and treated mice on day 27 post-inoculation. **B** Representative immunofluorescence images of $CD31^+$ vascular endothelial cells (red) counterstained with lectin (green) from LDRT treated tumors and size-matched control tumors at 3 h (0.1 day), 1 day, 4 days and 8 days post-RT. **C** Comparison of vessel perfusion (lectin covered $CD31^+$ cells) between 2 Gy × 5 fractions group and size-matched control group at different days following RT. **D** Representative immunofluorescence images of hypoxic ($pimonidazole^+$) area (green) for LDRT treated tumors and size-matched control tumors at 3 h (0.1 day), 1 day, 4 days and 8 days post-RT. **E** Comparison of hypoxic area between radiotherapy of 2 Gy × 5 fractions and size matched control groups at different days following RT. Representative immunofluorescence images of LDRT versus control tumors 1-day post-RT staining (in green) for **F** pericytes — alpha muscle smooth actin (aSMA); **G** pericyte maturation — caldesmon; **H** pericyte contractile ability — calponin; **I** endothelial cell activation—ICAM-1; and **J** vessel basement membrane — collagen IV. DAPI staining is blue and $CD31.^+$ is pink. NB: no data available for sham-irradiated animals at day 13 post-irradiation; tumors had already reached maximum size and mice had been euthanized. The experiment was repeated 4 times, with 1 mouse from each group and time point in each experimental repeat (n = 4 mice per group)

1-day post-irradiation generated the most differentially expressed genes (6378 total genes; 3532 upregulated and 2827 downregulated) (Fig. 5b). Pathway analysis demonstrated upregulation of interferon-γ, TNF-α, IL-2 signaling, inflammatory responses, T cell activation and migration, and MHC-I antigen presentation. Pathways such as DNA replication and repair, and G2/M cell cycle processes were downregulated (Fig. 5c–f). Whilst not in the top 500 upregulated pathways in the Gene Ontology pathway analysis, the 'regulation of angiogenesis' and 'positive regulation of angiogenesis' pathways were upregulated to a minor degree ($p = 0.026$ and $p = 0.0403$, respectively).

To better understand the immunological changes, the CIBERSORT algorithm was used to identify 25 immune cell types from gene expression data (Fig. 5g). This analysis highlighted differences in the predominant macrophage phenotype, with a prevalence of M0 (non-activated) macrophages in sham-irradiated tumors, and M1 (pro-inflammatory) macrophages in irradiated tumors. These differences appeared temporary and were minimal a week after irradiation (Fig. 5g and 5h). Non-significant differences in several other cell types as a proportion of total $CD45^+$ cells were also observed following CIBERSORT analysis (Supplementary Fig. 4). $CD8^+$ T cells appeared more abundant in LDRT tumors harvested 4 days post-irradiation than in sham-irradiated tumors, consistent with histological data. Natural killer cells also appeared proportionally higher in the LDRT group compared to the non-irradiated group at 0.1 days post-irradiation; however, there was no difference from day 1 to day 8. The proportion of B cells did not change between the LDRT and non-irradiated groups from 0.1 to 4 days; however, on day 8 it was lower in the LDRT group (Supplementary Fig. 4).

Post hoc analysis of normalized PD-1 and CTLA-4 mRNA expression indicated higher transcript levels from both genes in the LDRT group compared to the control group; however, it was only significant for 1-day post-irradiation (Supplementary Fig. 5).

Low-dose RT optimally improves response to immunotherapy when given concurrently

The combination anti-PD-1 (nivolumab) and anti-CTLA-4 (ipilimumab) is currently approved as first-line treatment for mesothelioma [2, 28]. However, most patients, especially those with epithelioid disease, do not respond to this combination and it is important to examine strategies to improve response rates. By treating tumors with LDRT (2 Gy × 5), we were able to transiently improve vascular function, enhance $\%sO_2$ levels, and increase the number of $CD8^+$ tumor-infiltrating lymphocytes (TILs) compared to controls. Based on these findings, we hypothesized that these changes could sensitize mesothelioma tumors to ICI therapy, and that this may require the delivery of immunotherapy to be appropriately timed with respect to irradiation.

Mice bearing subcutaneous AB1-HA mesothelioma tumors were treated with LDRT and/or dual ICIs, as shown in Fig. 6a. High complete response rates were observed in mice receiving dual ICIs either concurrently with LDRT (100%) or beginning 1 day after the final RT fraction (87.5%); this was more than double the cure rate seen in mice treated with dual ICIs without RT (43%) (Fig. 6b). However, there was only one complete response in irradiated mice that received dual ICIs starting 7 days post-irradiation (day 21 post-inoculation) (Fig. 6b). We observed a significant delay in tumor growth for mice treated dual ICIs concurrently with RT ($p = 0.014$) or 1 day after RT ($p = 0.027$) compared to dual ICIs. A significant delay in tumor growth was seen when comparing RT only with RT + dual ICIs concurrently ($p = 0.022$) and ICIs following RT ($p = 0.041$). There was no significant difference in tumor growth between treatment with dual ICIs only and RT only. All treatment groups had a significant delay in tumor growth compared to untreated mice (dual ICIs $p = 0.038$, RT $p = 0.027$, RT + dual ICIs (days 10, 12, 14) $p < 0.0001$, RT + dual ICIs (days 15, 17, 19) $p < 0.0001$, and RT + dual ICIs (days 21, 23, 25) $p = 0.002$; Fig. 6b). Median survival increased in all groups receiving RT + dual ICIs versus ICIs alone; however, this

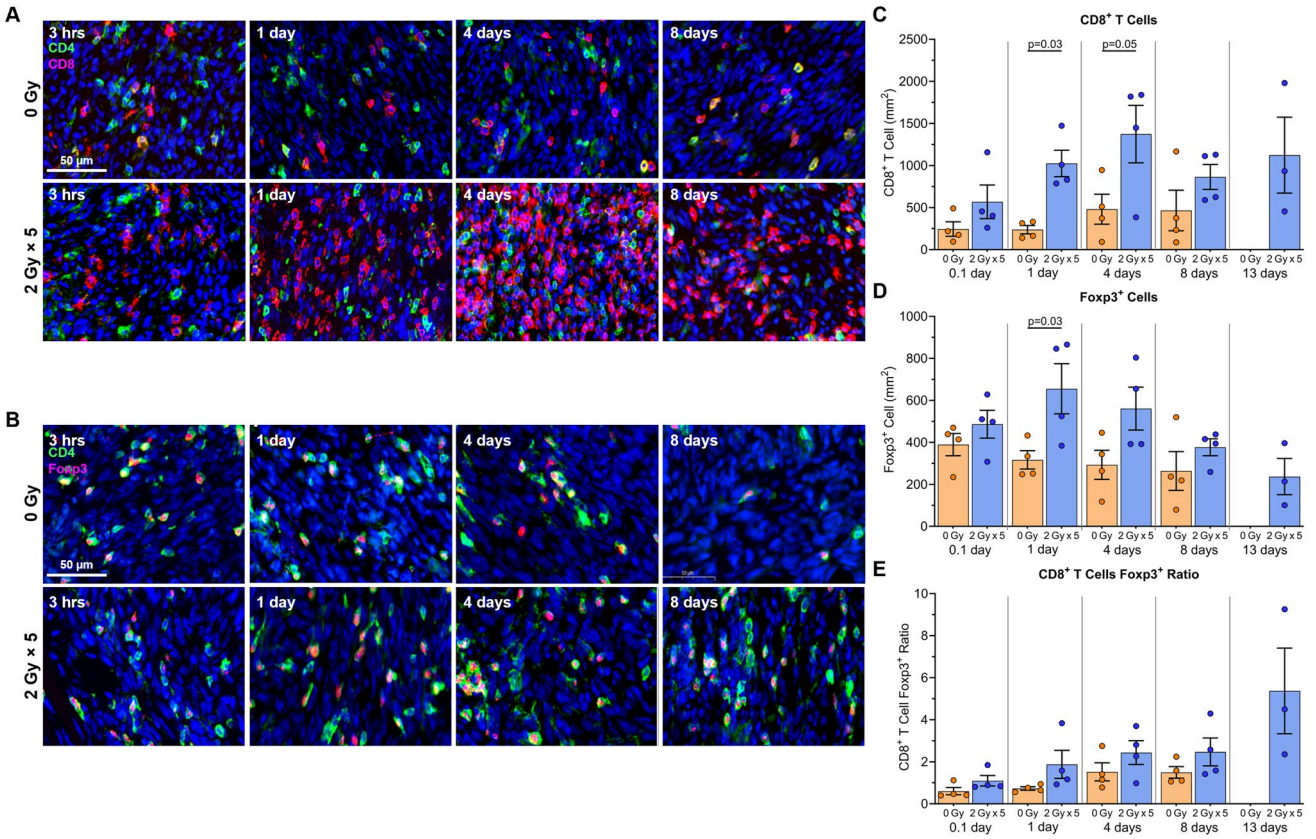

Fig. 4 LDRT induces significant cytotoxic T cell infiltration. Tumors were collected at sequential timepoints after RT for immunofluorescence staining. **A** Representative images of T cell subsets ($CD4^+$ — green, $CD8^+$ — red, nuclei (DAPI) — blue). **B** Representative images showing regulatory T cells ($CD4^+$ — green, $Foxp3^+$ — red, nuclei (DAPI) — blue). **C–E** Mean values plus individual data points showing **C** $CD8^+$ T cell concentration per mm^2, **D** $Foxp3^+$ Regulatory T cells concentration per mm^2, and **E** $CD8^+$ T cell to regulatory T cell ratio. Statistical significance was set at $p < 0.05$. The experiment was repeated 4 times, with 1 mouse from each group and time point in each experimental repeat (n = 4 mice per group)

was only significant for concurrent RT + ICIs ($p = 0.0217$; Fig. 6c). There was a significant increase in survival for mice treated with RT plus concurrent ($p = 0.00031$) or consecutive ($p = 0.00031$) dual ICIs compared to RT only. All treatment groups had a significant increase in survival compared to untreated mice (Fig. 6c).

Dual immunotherapies improve response rates; however, they increase the risk of adverse effects and toxicities in patients [2]. We investigated the effectiveness of anti-PD-1 combined with LDRT without the addition of anti-CTLA-4. Mice were treated with LDRT and/or anti-PD-1, as shown in Fig. 6a. A complete response was observed in 55% of mice that received concurrent RT + anti-PD-1, and the cure rates decreased the later after RT the anti-PD-1 treatment began (Fig. 6d). All RT + anti-PD-1 treatment groups had a significant delay in tumor growth compared to anti-PD-1 only ($p = 0.005$, $p = 0.012$, and $p = 0.032$ for each group respectively). There was no significant growth delay between RT only and anti-PD-1 only, and RT only with any of the RT + anti-PD-1 treatment groups (Fig. 6d). All treatment groups, except anti-PD-1 only, had a significant delay in tumor growth compared to untreated mice (anti-PD-1 $p = 0.653$, RT $p = 0.007$, RT + anti-PD-1 (days 10, 12, 14) $p < 0.0001$, RT + anti-PD-1 (days 15, 17, 19) $p = 0.0002$, and RT + anti-PD-1 (days 21, 23, 25) $p = 0.002$; Fig. 6d). There was an increase in median survival for RT + anti-PD-1 treatments compared to anti-PD-1 only; however, survival was only significantly increased when anti-PD-1 was given concurrently with or 1 day after RT ($p = 0.027$ and $p = 0.034$ respectively; Fig. 6e). There was a non-significant increase in median survival for RT + anti-PD-1 treatments compared to RT only. All treatment groups had a significant increase in survival compared to untreated mice (Fig. 6e).

The addition of anti-CTLA-4 significantly increased the survival rate for RT + ICI schedules when ICIs were given with or 1 day after RT ($p = 0.0369$ and $p = 0.0069$ respectively), but not for the later delivery of ICIs ($p = 0.340$) or ICIs alone ($p = 0.221$).

Cured mice (no primary tumor for 30 days) underwent tumor rechallenge on the opposite flank, with no

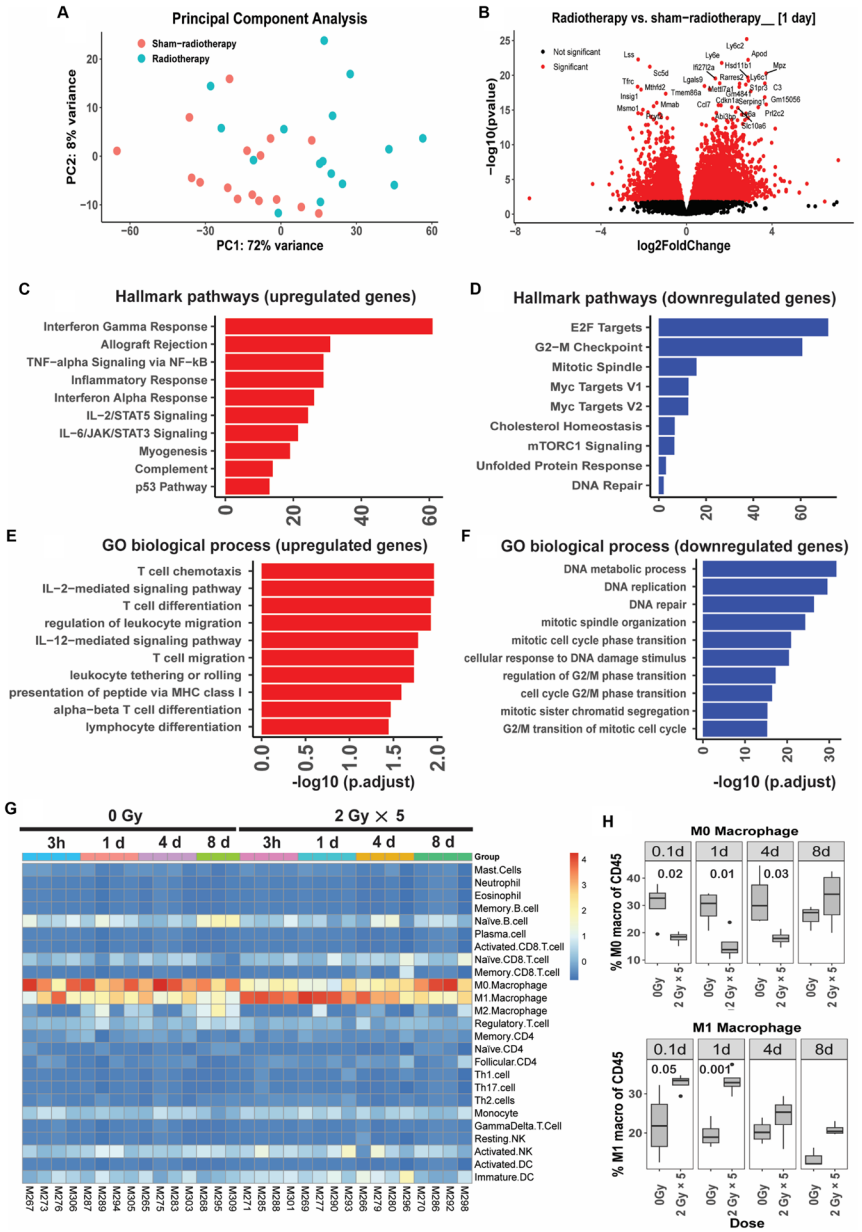

Fig. 5 LDRT induces a significant number of differentially expressed genes. **A** Principal component analysis of RNA transcript data revealing separation between radiotherapy versus sham-irradiation groups. **B** Volcano plot demonstrating 6378 differentially expressed genes in response to LDRT, in comparison to sham-irradiation, 1 day following final RT (3532 genes upregulated and 2827 genes downregulated). **C** and **D** Hallmark pathway, and **E** and **F** Gene Ontology (biological process) pathway analysis, showing top 10 upregulated (red) and downregulated (blue) gene sets for each. **G** Supervised hierarchical clustering of innate and adaptive immune cells as estimated by CIBERSORT algorithm, revealing separation of M1 and M0 macrophages between radiotherapy and sham-radiotherapy. **H** Proportion of M1 and M0 macrophages estimated by CIBERSORT across experimental time-course. Independent T test for two group comparison. The experiment was repeated 4 times, with 1 mouse from each group and time point in each experimental repeat (n = 4 mice per group)

reinoculated animals developing secondary tumors, indicating immunological protection. One primary tumor relapsed in the RT + anti-PD-1 + anti-CTLA-4 (days 15, 17 and 19) group after a period of 30 days with no measurable primary tumor; interestingly, this relapse occurred one week following rechallenge. Taken together, these indicate that efficacy of concurrent RT + anti-PD-1 + anti-CTLA-4 is superior to delayed ICIs, suggesting timing of immunotherapy administration with respect to RT is crucial for optimal synergy.

Discussion

ICIs have been approved for clinical use in a growing number of cancer types; however, only a minority of patients respond. Consequently, there is an urgent need for strategies to unlock the full potential of ICIs. In this study, the hypothesis was posited that a low number of fractions of the conventional dose of 2 Gy, resulting in a low total dose

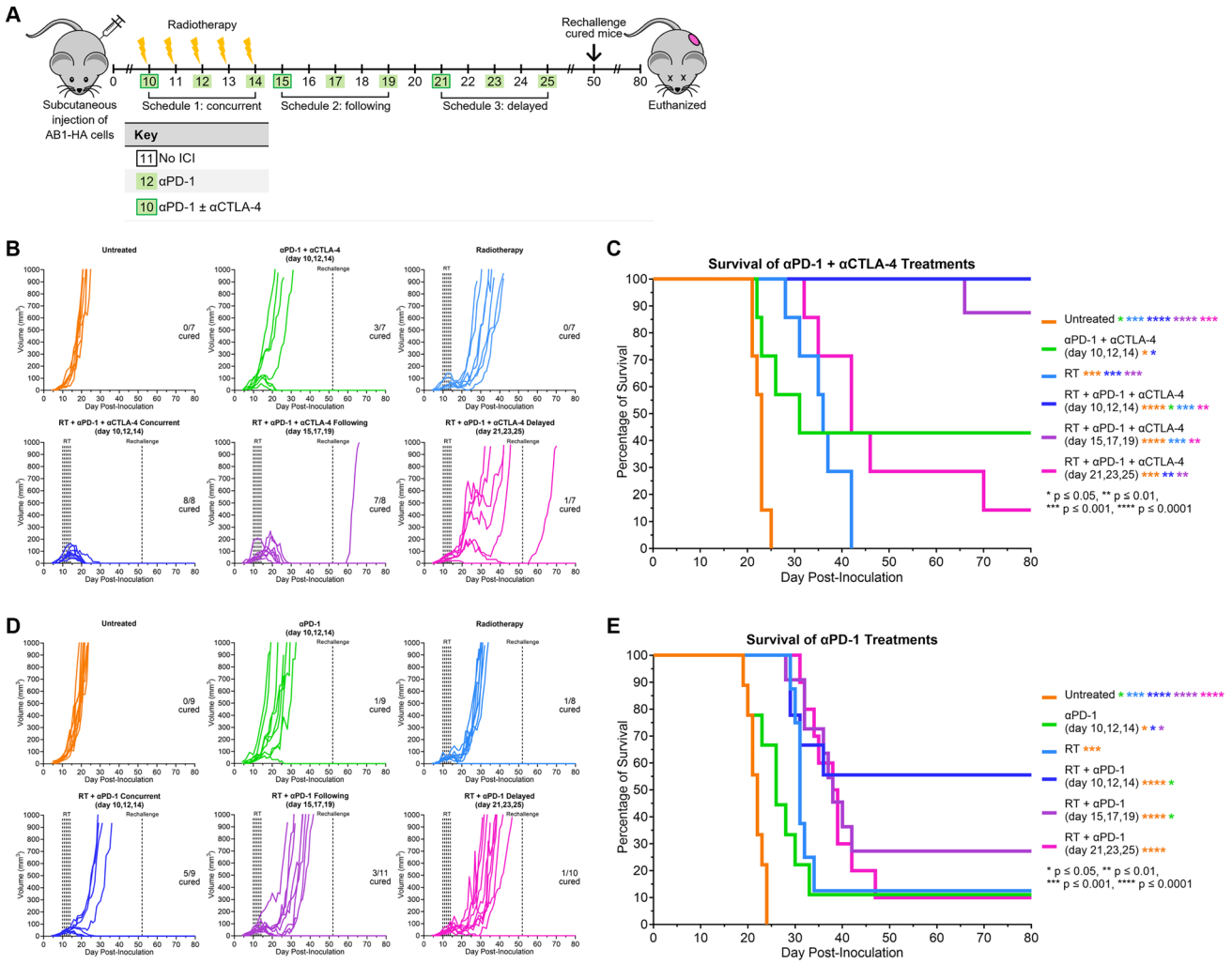

Fig. 6 LDRT treatment improves response to anti-PD-1 and anti-CTLA-4. **A** Schematic timeline showing radiotherapy-immunotherapy schedules. Subcutaneous injection of AB1-HA cells occurred on day 0. Radiotherapy commenced on day 10 post-inoculation, when tumors were ~ 40 ± 15 mm^3. Tumors were irradiated with 2 Gy for 5 consecutive days. Immunotherapy was administered over 3 injections as described. Mice were monitored for up to 80 days and euthanized if tumors reached 1000 mm^3. **B** Individual tumor growth curves for each treatment group with anti-PD-1 and anti-CTLA-4, numbers inset on plots represent 'cured mice'/'total mice in group'. **C** Kaplan-Meier survival curves for all treatment groups with anti-PD-1 and anti-CTLA-4. **D** Individual tumor growth curves for each treatment group with anti-PD-1, numbers inset on plots represent 'cured mice'/'total mice in group'. **E** Kaplan-Meier survival curves for all treatment groups with anti-PD-1. Asterisks indicate significance between groups as indicated by color. $*p<0.05$, $**p<0.01$, $***p<0.001$, $****p<0.0001$. Each experiment was repeated 3 times, with 2 to 4 mice from each group in each experimental repeat

(LDRT), could modulate tumor vasculature, priming the TME to enhance ICI efficacy. The validity of our approach was confirmed using advanced imaging techniques, along with phenotypic and functional studies in a well-characterized preclinical model of mesothelioma. Existing literature on this topic presents conflicting findings, with studies in various cancer models suggesting that both low and hypofractionated doses of RT might normalize tumor vessels [10, 11, 21, 43].

After exploring temporal changes in tumor blood flow and oxygen saturation in vivo for multiple dose fractionation schedules, a distinct additive effect when administering multiple consecutive daily fractions was demonstrated. The standard dose used in human treatment (2 Gy per fraction) was specifically chosen, as higher hypofractionated doses have been found to cause damage to blood vessels [8, 10, 12, 13]. Crucially, fewer RT fractions (five) were delivered compared with previous studies on vascular remodeling, which utilized up to 10 fractions of 2 Gy [10]. Therefore, our approach may result not only in lower tissue toxicity, but also fewer logistical challenges for the preclinical setting and for future translation. Less RT fractions would also reduce the impact on patients, as there are fewer treatment days compared to conventional RT schedules.

Increased pericyte coverage around tumor vessels following LDRT has been consistently observed and reported in response to a wide range of RT doses in previous studies [10, 11, 21, 43]. Vascular modification following LDRT was shown to be transient and coincides with several immune-related changes, including increased intra-tumoral $CD8^+$ T cell concentration. Similar findings were reported in a previous study which demonstrated an increase in $CD3^+CD8^+$ T cells in AB12 and AE17 mesothelioma tumor models on day 7, peaking at day 12 after RT, with a fractionation schedule of 5 Gy × 3 fractions [18]. The increased T cell population is considered most likely due to an influx of infiltrating cells through the modified, more functional vasculature, rather than the proliferation of a small number of pre-existing TILs. This is supported by our observation of increased ICAM-1 expression (necessary for the leukocyte adhesion cascade, including capture, rolling and transmigration) 1-day post-irradiation [8]. Apart from observing heavily upregulated genes associated with inflammatory response pathways following LDRT, as previously reported by other studies [15, 16], downregulated genes were also found to be over-represented in DNA repair, DNA replication, and regulation of G2/M phase. These could contribute to the delays in tumor growth following LDRT in our model. With respect to the apparent polarization from M0 (resting) toward M1 (inflammatory) macrophage phenotypes, our findings align with several previous studies demonstrating that LDRT (0.5–2 Gy) increased the presence of M1 macrophages [44–46]. In previous murine studies, it was also reported that LDRT schedules of 2 Gy × 2 fractions suppressed p38 mitogen-activated protein-inducing M1 acquisition, accompanied by reduction in M2 macrophage associated proteins such as Ym-1, Fizz-1, Arginase-1 and HSP90 in irradiated mice [45]. Another study reported that switching from M2 to M1 was due to a reduction in tumor hypoxia [46]. The accumulation of M1 macrophage may also increase the efficacy of ICIs.

The 'hot' or 'cold' nature of tumors, as with most biological systems, is not binary but a spectrum. Whilst this tumor model is in the 'colder' end of this spectrum, there appears to be a 'tipping point' beyond which tumors can successfully respond to therapy [47], as some unirradiated tumors responded to ICIs alone. The nature of this tipping point for this tumor model cannot be conclusively determined from these experiments, however, it can be speculated that the immune infiltrate is a factor, particularly the levels of tumor specific $CD8^+$ T cells. Immunofluorescent staining showed a range of TIL concentrations present in untreated tumors, and it is possible that responders to ICIs had more $CD8^+$ TIL populations. This would be supported by clinical literature, where $CD8^+$ T cell infiltration has been reported to positively correlate with ICI outcomes in several cancers [48–50]. This suggests our LDRT strategy can change tumors toward the 'hot' end of the spectrum and thus increases the proportion that are beyond the tipping point where a response to ICIs is now achievable.

While studies combining RT with ICIs have reported promising results for mesothelioma treatment both in clinical and preclinical settings, our study is the first to specifically target the vasculature with RT to improve current standard-care immunotherapy [18, 27, 51, 52]. Our study used a well-characterized mesothelioma model, which demonstrated variable responses to either anti-PD-1 monotherapy or combined anti-PD1 and anti-CTLA-4, with better responses seen for the ICI combination. Not all mice responded to ICIs, therefore, our model replicates the clinical settings, where some patients did not respond to immunotherapy. Consistent and reliable complete responses were achieved in mice treated with combined LDRT and first-line ICIs for mesothelioma (anti-PD-1 plus anti-CTLA-4). Our findings align with previous radiotherapy-immunotherapy studies, demonstrating higher complete response rates when RT was combined with dual ICIs compared to RT alone, ICI monotherapy, or RT plus ICI monotherapy [14–17, 20, 53]. These findings suggest that the key to improving overall survival and inducing durable and complete responses lies in blocking the inhibition steps imposed on T cells during the priming phase (anti-CTLA-4) and in peripheral tissue (anti-PD-1). Importantly, treatment achieved the highest success when ICIs were administered concurrently with or immediately after LDRT. This aligns with our identification of a defined vascular modulation temporal window. One explanation is that once PD-1/PD-L1 engagement occurs within the tumor, it rapidly inhibits T cell activity. Prolonged signaling leads to a 'terminally exhausted' phenotype that is unlikely to be reversed by a subsequent anti-PD-1 blockade [54]. However, if cells receive anti-PD-1 blockade at an early stage or are 'pre-blocked' prior to tumor entry, their functionality can be maintained.

Conclusion

This study shows that LDRT, delivered in 2 Gy × 5 fractions, can create a tumor environment that is more conducive to the success of ICIs. LDRT can remodel vasculature to improve perfusion, reduces hypoxia, and increases the presence of perivascular structural and functional components. These changes, accompanied by increased $CD8^+$ T cells and an upregulation of pro-inflammatory pathways, may be particularly useful in modifying the microenvironment of immunologically 'cold' tumors. Since the immunotherapies studied are regularly used to treat mesothelioma, it should soon be possible to clinically assess LDRT + ICIs.

Supplementary Information The online version contains supplementary material available at https://doi.org/10.1007/s00262-024-03889-x.

Acknowledgements The authors acknowledge the facilities and scientific and technical assistance offered, at the Centre for Microscopy, Characterisation and Analysis, University of Western Australia, with special thanks to Diana Patalwala and Ivan Lozić. The authors acknowledge the facilities and scientific and technical assistance offered at the Telethon Kids Institute, with special thanks to Blake Klyen and Tamara Abel. Rebecca D'Alonzo was supported by the Sir Charles Gairdner Hospital Radiation Oncology Scholarship in Radiobiology. Synat Keam was supported by a University of Western Australia International PhD Scholarship and the Peter Douglas Swift PhD top-up scholarship. The National Centre for Asbestos Related Diseases was supported by the National Health and Medical Research Council with a Centre of Research Excellence grant, application ID: APP1197652. This study was supported by grant 1163065 from the Cancer Australia Priority-driven Collaborative Cancer Research Scheme. The contents are solely the responsibility of the individual authors and do not reflect the views of Cancer Australia.

Author contributions Conceptualization: MAE, AMC, AKN. Methodology: MAE, AMC, RAD, SK. Investigation: RAD, SK. Data curation: RAD, SK. Formal Analysis: RAD, SK. Visualization: RAD, SK. Funding acquisition: MAE, AMC, AKN, SG. Project administration: MAE, AMC. Supervision: MAE, AMC, PR SG, AKN. Writing — original draft: RAD, SK. Writing — review and editing: RAD, SK, MAE, AMC, SG, PR, AKN.

Funding This work was supported by the National Health & Medical Research Council with a Centre of Research Excellence grant APP1197652 (ANK, AMC), the Cancer Australia Priority-driven Collaborative Cancer Research Scheme grant 1163065 (MAE, AMC, AKN, SG), the Mesothelioma Applied Research Foundation grant (AMC), and the iCare Dust Diseases Board Fellowship (AMC).

Data availability The data generated in this study are available upon request from the corresponding author.

Declarations

Conflict of interest The authors declare no conflict of interest.

Ethical approval All experimental protocols involving mice were approved by the Animal Ethics Committees of HPIMR, the University of Western Australia (UWA), and the Telethon Kids Institute (Perth, Australia) (AE163) and were conducted in accordance with the Australian Code for the Care and Use of Animals for Scientific Purposes (8th edition, 2013) and UWA animal ethics guidelines and protocols.

References

1. Esfahani K et al (2020) A review of cancer immunotherapy: from the past, to the present, to the future. Curr Oncol 27:S87–S97. https://doi.org/10.3747/co.27.5223
2. Nowak AK, Chin WL, Keam S, Cook A (2021) Immune checkpoint inhibitor therapy for malignant pleural mesothelioma. Lung Cancer 162:162–168. https://doi.org/10.1016/j.lungcan.2021.11.006
3. Nowak AK, Brosseau S, Cook A, Zalcman G (2020) Antiangiogeneic strategies in mesothelioma. Front. Oncol 10:126. https://doi.org/10.3389/fonc.2020.00126
4. Vaupel P (2004) Tumor microenvironmental physiology and its implications for radiation oncology. Semin Radiat Oncol 14(3):198. https://doi.org/10.1016/j.semradonc.2004.04.008
5. Liu Z et al (2021) Vascular normalization in immunotherapy: a promising mechanisms combined with radiotherapy. Biomed Pharmacother 139:111607. https://doi.org/10.1016/j.biopha.2021.111607
6. Abou Khouzam R et al (2020) Tumor hypoxia regulates immune escape/invasion: influence on angiogenesis and potential impact of hypoxic biomarkers on cancer therapies. Front Immunol 11:613114. https://doi.org/10.3389/fimmu.2020.613114
7. Donlon NE, Power R, Hayes C, Reynolds JV, Lysaght J (2021) Radiotherapy, immunotherapy, and the tumor microenvironment: turning an immunosuppressive milieu into a therapeutic opportunity. Cancer Lett 502:84–96. https://doi.org/10.1016/j.canlet.2020.12.045
8. Yamazaki T, Young KH (2022) Effects of radiation on tumor vasculature. Mol Carcinog 61:165–172. https://doi.org/10.1002/mc.23360
9. Kleibeuker EA et al (2016) Low dose angiostatic treatment counteracts radiotherapy-induced tumor perfusion and enhances the anti-tumor effect. Oncotarget 7:76613–76627. https://doi.org/10.18632/oncotarget.12814
10. Clément-Colmou K et al (2020) Influence of radiotherapy fractionation schedule on the tumor vascular microenvironment in prostate and lung cancer models. Cancers (Basel) 12:12. https://doi.org/10.3390/cancers12010121
11. Potiron V et al (2019) Tumor vasculature remodeling by radiation therapy increases doxorubicin distribution and efficacy. Cancer Lett 457:1–9. https://doi.org/10.1016/j.canlet.2019.05.005
12. Arnold KM et al (2018) The impact of radiation on the tumor microenvironment: effect of dose and fractionation schedules. Cancer Growth Metastasis. https://doi.org/10.1177/1179064418761639
13. Goedegebuure RSA, de Klerk LK, Bass AJ, Derks S, Thijssen VLJL (2018) Combining radiotherapy with anti-angiogenic therapy and immunotherapy; a therapeutic triad for cancer? Front Immunol 9:3107. https://doi.org/10.3389/fimmu.2018.03107
14. Barsoumian HB et al (2020) Low-dose radiation treatment enhances systemic antitumor immune responses by overcoming the inhibitory stroma. J Immunother Cancer 8:2. https://doi.org/10.1136/jitc-2020-000537
15. Patel RB et al (2021) Low-dose targeted radionuclide therapy renders immunologically cold tumors responsive to immune checkpoint blockade. Sci Transl Med. https://doi.org/10.1126/scitranslmed.abb3631
16. Herrera FG et al (2022) Low-dose radiotherapy reverses tumor immune desertification and resistance to immunotherapy. Cancer Discov 12:108–133. https://doi.org/10.1158/2159-8290.CD-21-0003
17. Murakami J et al (2021) Triple-modality therapy maximizes antitumor immune responses in a mouse model of mesothelioma. Sci Transl Med. https://doi.org/10.1126/scitranslmed.abd9882

18. De La Maza L et al (2017) In situ vaccination after accelerated hypofractionated radiation and surgery in a mesothelioma mouse model. Clin Cancer Res 23:5502–5513. https://doi.org/10.1158/1078-0432.CCR-17-0438
19. Keam S, Gill S, Ebert MA, Nowak AK, Cook AM (2020) Enhancing the efficacy of immunotherapy using radiotherapy. Clin Transl Immunology 9:e1169. https://doi.org/10.1002/cti2.1169
20. Dovedi SJ et al (2014) Acquired resistance to fractionated radiotherapy can be overcome by concurrent PD-L1 blockade. Cancer Res 74:5458–5468. https://doi.org/10.1158/0008-5472.CAN-14-1258
21. Potiron VA et al (2013) Improved functionality of the vasculature during conventionally fractionated radiation therapy of prostate cancer. PLoS ONE 8:e84076. https://doi.org/10.1371/journal.pone.0084076
22. Gil Marques F et al (2019) Low doses of ionizing radiation activate endothelial cells and induce angiogenesis in peritumoral tissues. Radiother Oncol 141:256–261. https://doi.org/10.1016/j.radonc.2019.06.035
23. Hohlweg-Majert B et al (2012) Impact of radiotherapy on microsurgical reconstruction of the head and neck. J Cancer Res Clin Oncol 138:1799–1811. https://doi.org/10.1007/s00432-012-1263-6
24. Patel RR et al (2021) High-dose irradiation in combination with non-ablative low-dose radiation to treat metastatic disease after progression on immunotherapy: results of a phase II trial. Radiother Oncol 162:60–67. https://doi.org/10.1016/j.radonc.2021.06.037
25. Dewan MZ et al (2009) Fractionated but not single-dose radiotherapy induces an immune-mediated abscopal effect when combined with anti-CTLA-4 antibody. Clin Cancer Res 15:5379–5388. https://doi.org/10.1158/1078-0432.CCR-09-0265
26. Demaria S et al (2021) Radiation dose and fraction in immunotherapy: one-size regimen does not fit all settings, so how does one choose? J Immunother.Cancer 9:e002038. https://doi.org/10.1136/jitc-2020-002038
27. Wu L et al (2015) Targeting the inhibitory receptor CTLA-4 on T cells increased abscopal effects in murine mesothelioma model. Oncotarget 6:12468–12480. https://doi.org/10.18632/oncotarget.3487
28. Baas P et al (2021) First-line nivolumab plus ipilimumab in unresectable malignant pleural mesothelioma (CheckMate 743): a multicentre, randomised, open-label, phase 3 trial. Lancet 397:375–386. https://doi.org/10.1016/S0140-6736(20)32714-8
29. Davis MR, Manning LS, Whitaker D, Garlepp MJ, Robinson BW (1992) Establishment of a murine model of malignant mesothelioma. Int J Cancer 52:881–886. https://doi.org/10.1002/ijc.2910520609
30. Jackaman C et al (2003) IL-2 intratumoral immunotherapy enhances CD8+ T cells that mediate destruction of tumor cells and tumor-associated vasculature: a novel mechanism for IL-2. J Immunol 171:5051–5063. https://doi.org/10.4049/jimmunol.171.10.5051
31. Marzo AL, Lake RA, Robinson BW, Scott B (1999) T-cell receptor transgenic analysis of tumor-specific CD8 and CD4 responses in the eradication of solid tumors. Cancer Res 59:1071–1107
32. Ma CM et al (2001) AAPM protocol for 40–300 kV x-ray beam dosimetry in radiotherapy and radiobiology. Med Phys 28:868–893. https://doi.org/10.1118/1.1374247
33. Feddersen TV, Rowshanfarzad P, Abel TN, Ebert MA (2019) Commissioning and performance characteristics of a pre-clinical image-guided radiotherapy system. Australas Phys Eng Sci Med 42:541–551. https://doi.org/10.1007/s13246-019-00755-4
34. Bray NL, Pimentel H, Melsted P, Pachter L (2016) Near-optimal probabilistic RNA-seq quantification. Nat Biotechnol 34:525–527. https://doi.org/10.1038/nbt.3519
35. Soneson C, Love MI, Robinson MD (2015) Differential analyses for RNA-seq: transcript-level estimates improve gene-level inferences. F1000Research 30(4):1521. https://doi.org/10.12688/f1000research.7563.2
36. Love MI, Huber W, Anders S (2014) Moderated estimation of fold change and dispersion for RNA-seq data with DESeq2. Genome Biol 15:550. https://doi.org/10.1186/s13059-014-0550-8
37. Chen EY et al (2013) Enrichr: interactive and collaborative HTML5 gene list enrichment analysis tool. BMC Bioinfo 14:128. https://doi.org/10.1186/1471-2105-14-128
38. Chen B, Khodadoust MS, Liu CL, Newman AM, Alizadeh AA (2018) Profiling tumor infiltrating immune cells with CIBERSORT. Methods Mol Biol 1711:243–259. https://doi.org/10.1007/978-1-4939-7493-1_12
39. Chen Z et al (2017) Inference of immune cell composition on the expression profiles of mouse tissue. Sci Rep 7:40508. https://doi.org/10.1038/srep40508
40. Dupont WD, Plummer WD Jr (1998) Power and sample size calculations for studies involving linear regression. Control Clin Trials 19(6):589–601. https://doi.org/10.1016/s0197-2456(98)00037-3
41. D'Alonzo RA et al (2021) In vivo noninvasive preclinical tumor hypoxia imaging methods: a review. Int J Radiat Biol 97:593–631. https://doi.org/10.1080/09553002.2021.1900943
42. He B et al (2020) Remodeling of metastatic vasculature reduces lung colonization and sensitizes overt metastases to immunotherapy. Cell Rep 30:714-724.e5. https://doi.org/10.1016/j.celrep.2019.12.013
43. Lan J et al (2013) Ablative hypofractionated radiotherapy normalizes tumor vasculature in lewis lung carcinoma mice model. Radiat Res 179:458–464. https://doi.org/10.1667/RR3116.1
44. Klug F et al (2013) Low-dose irradiation programs macrophage differentiation to an iNOS$^+$/M1 phenotype that orchestrates effective T cell immunotherapy. Cancer Cell 24:589–602. https://doi.org/10.1016/j.ccr.2013.09.014
45. Prakash H et al (2016) Low doses of gamma irradiation potentially modifies immunosuppressive tumor microenvironment by retuning tumor-associated macrophages: lesson from insulinoma. Carcinogenesis 37:301–313. https://doi.org/10.1093/carcin/bgw007
46. Nadella V et al (2018) Low dose radiation primed iNOS + M1macrophages modulate angiogenic programming of tumor derived endothelium. Mol Carcinog 57:1664–1671. https://doi.org/10.1002/mc.22879
47. Creemers JHA, Lesterhuis WJ, Mehra N et al (2021) A tipping point in cancer-immune dynamics leads to divergent immunotherapy responses and hampers biomarker discovery. J Immunother Cancer 30(4):877–882. https://doi.org/10.1136/jitc-2020-002032
48. Dejardin D, Kraxner A, Blank A, Rieder N, Teichgräber V et al (2024) A composite decision rule of CD8+ T-cell density in tumor biopsies predicts efficacy in early-stage. Immunother Trials Clin Cancer Res 30(4):877–882. https://doi.org/10.1158/1078-0432.CCR-23-1572
49. Li F, Li C, Cai X, Xie Z, Zhou L, Cheng B et al (2021) The association between CD8+ tumor-infiltrating lymphocytes and the clinical outcome of cancer immunotherapy: a systematic review and meta-analysis. EClinicalMedicine 16(41):101134. https://doi.org/10.1016/j.eclinm.2021.101134
50. Hashemi S, Fransen MF, Niemeijer A, Ben Taleb N, Houda I, Veltman J et al (2021) Surprising impact of stromal TIL's on immunotherapy efficacy in a real-world lung cancer study. Lung Cancer 1(153):81–89. https://doi.org/10.1016/j.lungcan.2021.01.013
51. Mampuya WA et al (2021) Abscopal effect in a patient with malignant pleural mesothelioma treated with palliative radiotherapy and pembrolizumab. Clinical Trans Radiat Oncol 27:85–88. https://doi.org/10.1016/j.ctro.2020.12.006

52. Rittberg R, Chan E, Yip S, Alex D, Ho C (2022) Radiation induced abscopal effect in a patient with malignant pleural mesothelioma on pembrolizumab. Cureus. https://doi.org/10.7759/cureus.22159
53. Kim JE et al (2017) Combination therapy with anti-PD-1, Anti-TIM-3, and focal radiation results in regression of murine gliomas. Clin Cancer Res 23:124–136. https://doi.org/10.1158/1078-0432.CCR-15-1535
54. Dolina JS, Van Braeckel-Budimir N, Thomas GD, Salek-Ardakani S (2021) CD8+ T cell exhaustion in cancer. Front Immunol 12:715234. https://doi.org/10.3389/fimmu.2021.715234